ЛОБАЧЕВСКИЙ AI

Центр искусственного интеллекта ННГУ

«Патологические маркеры в интериктальной ЭЭГ»

Мальков А.Е., Лебедева А.В., Герасимова С.А., Леванова Т.А., Смирнов Л.А., Писарчик А.Н.

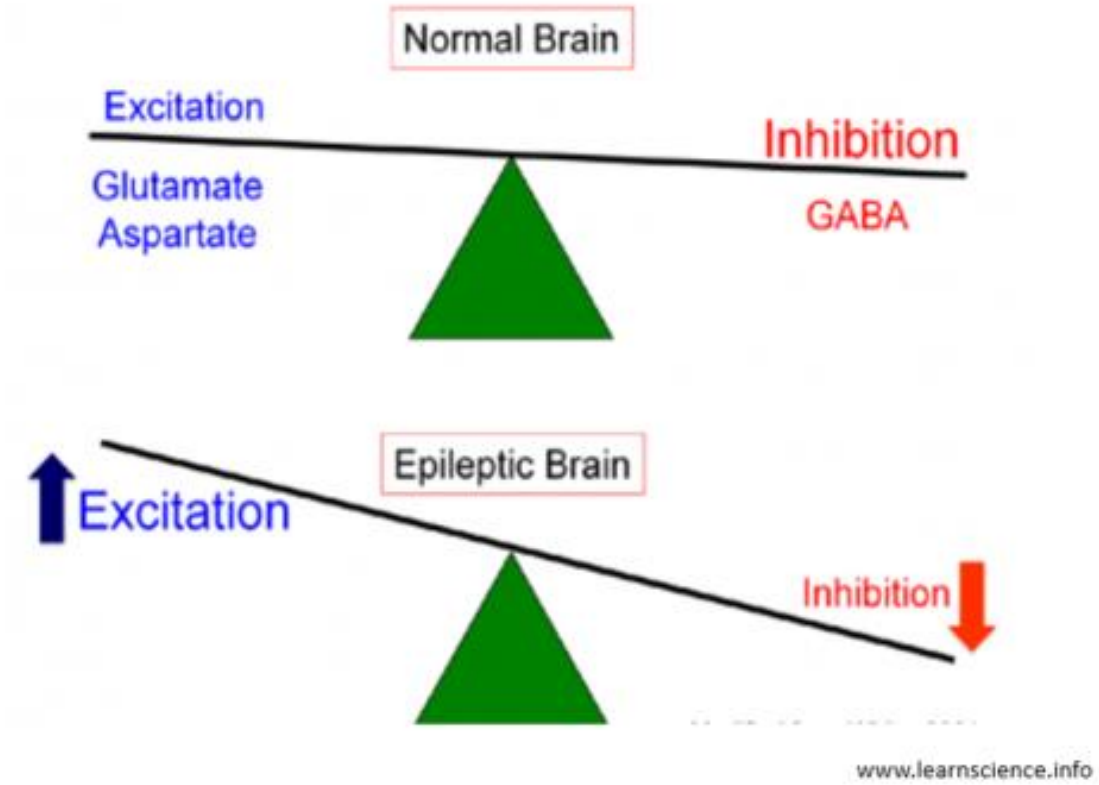
Normal Brain
Excitation
Inhibition
Glutamate
Aspartate
GABA
Epileptic Brain
Excitation
Inhibition
www.learnscience.info

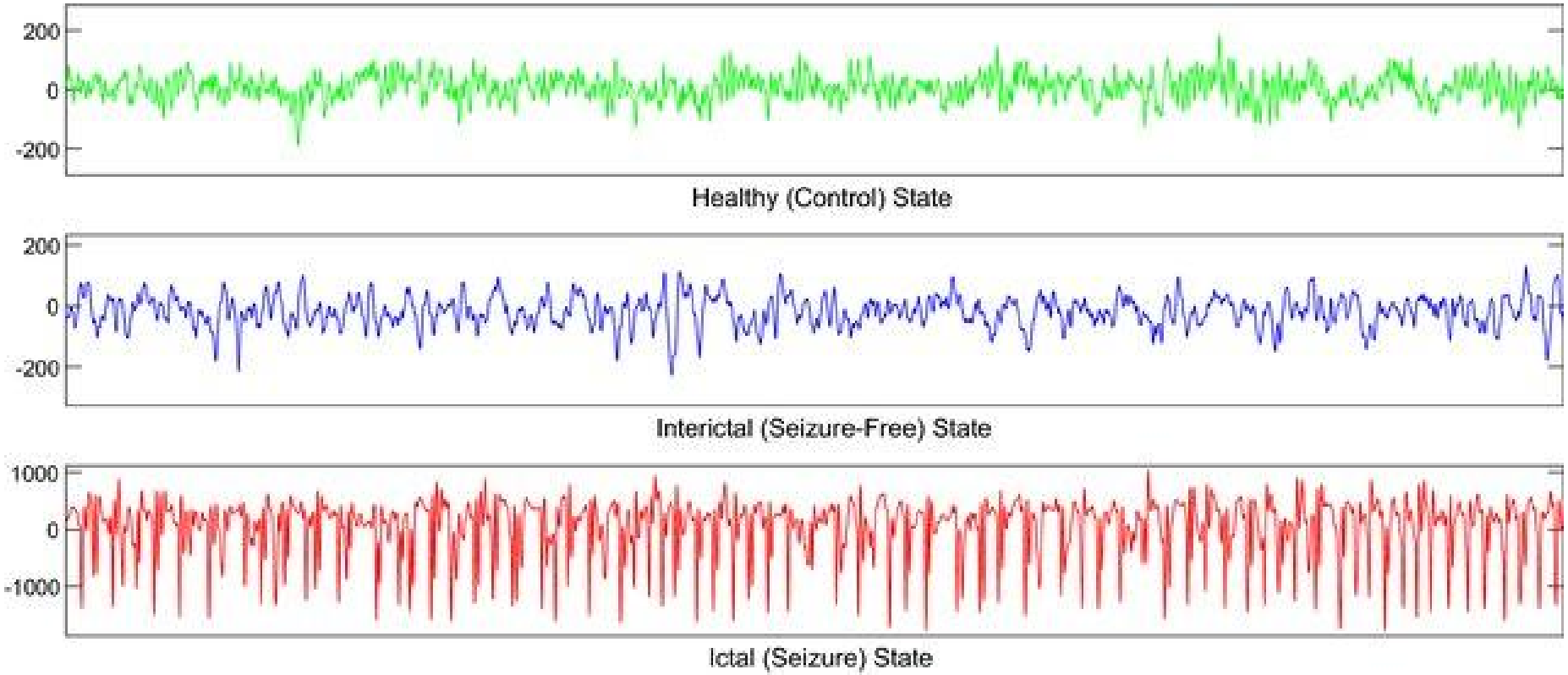
200
0
-200
Healthy (Control) State
200
0
-200
Interictal (Seizure-Free) State
1000
0
-1000
Ictal (Seizure) State

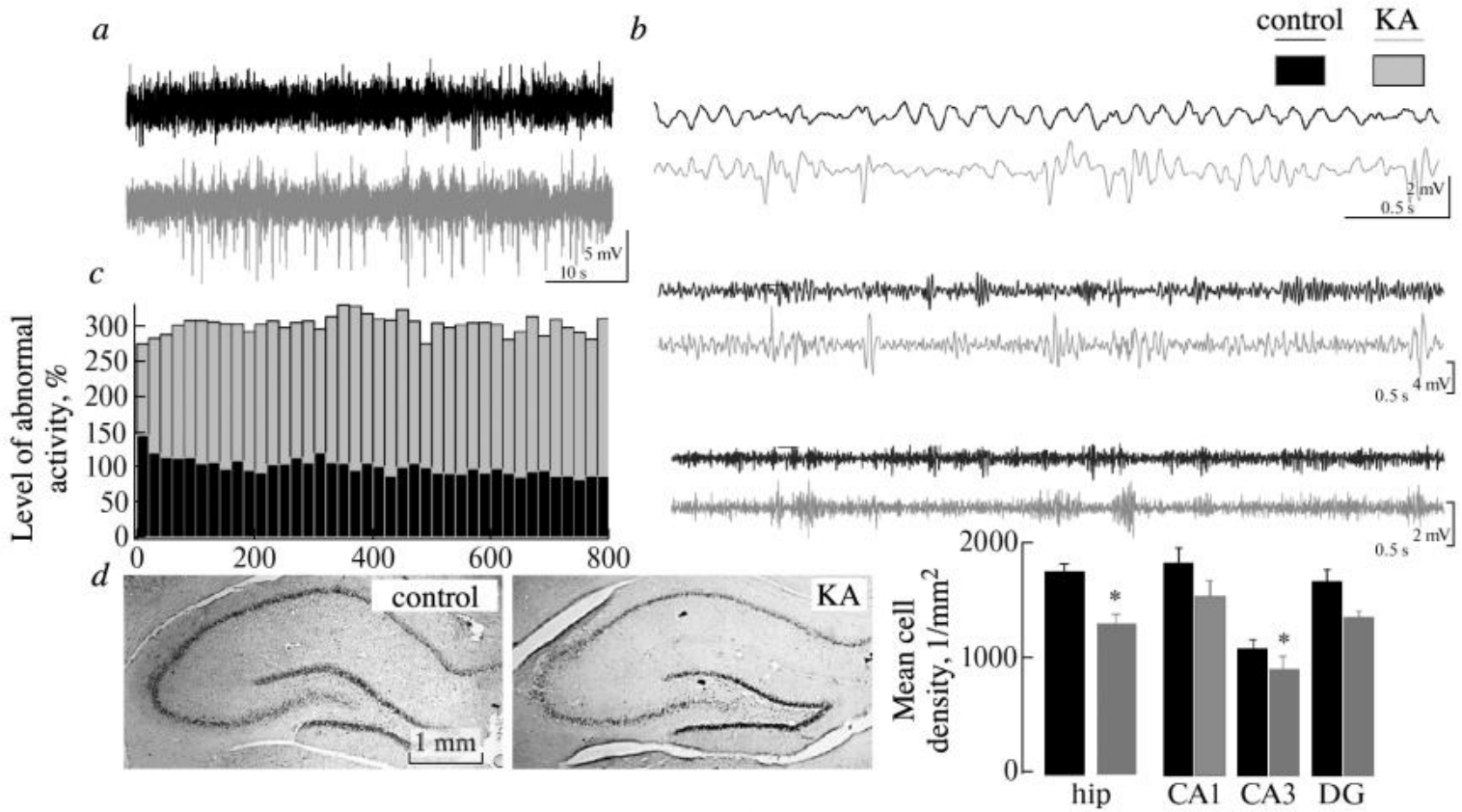

Fig. 2. Changes in the field activity and state of hippocampal tissues in the model of kainate neurotoxicity. *a*) Examples of recorded hippocampal LFP from healthy animals (controls) and in the model of kainate neurotoxicity (KA). Animals with the kainate neurotoxicity model displayed frequent high-amplitude paroxysmal events. *b*) Examples of LFP (same as in *a*) filtered in the θ (4–10 Hz, above), slow γ (25–50 Hz, middle), and fast γ (55–100 Hz, below) ranges. *c*) Total level of anomalous activity, all animals – integral of all high-amplitude (>3SD) events in hippocampal LFP. The level in controls was taken as 100%. *d*) Examples of frontal sections of the hippocampus stained by the Nissl method. Left: sections including all hippocampal fields and the dentate fascia in controls and after administration of kainic acid (KA); right: histogram showing mean cell density in the hippocampus as a whole (hip) and in separate parts of the hippocampus (CA1, CA3, DG); significant changes in cell numbers in field CA3 (*$p = 0.0483$).

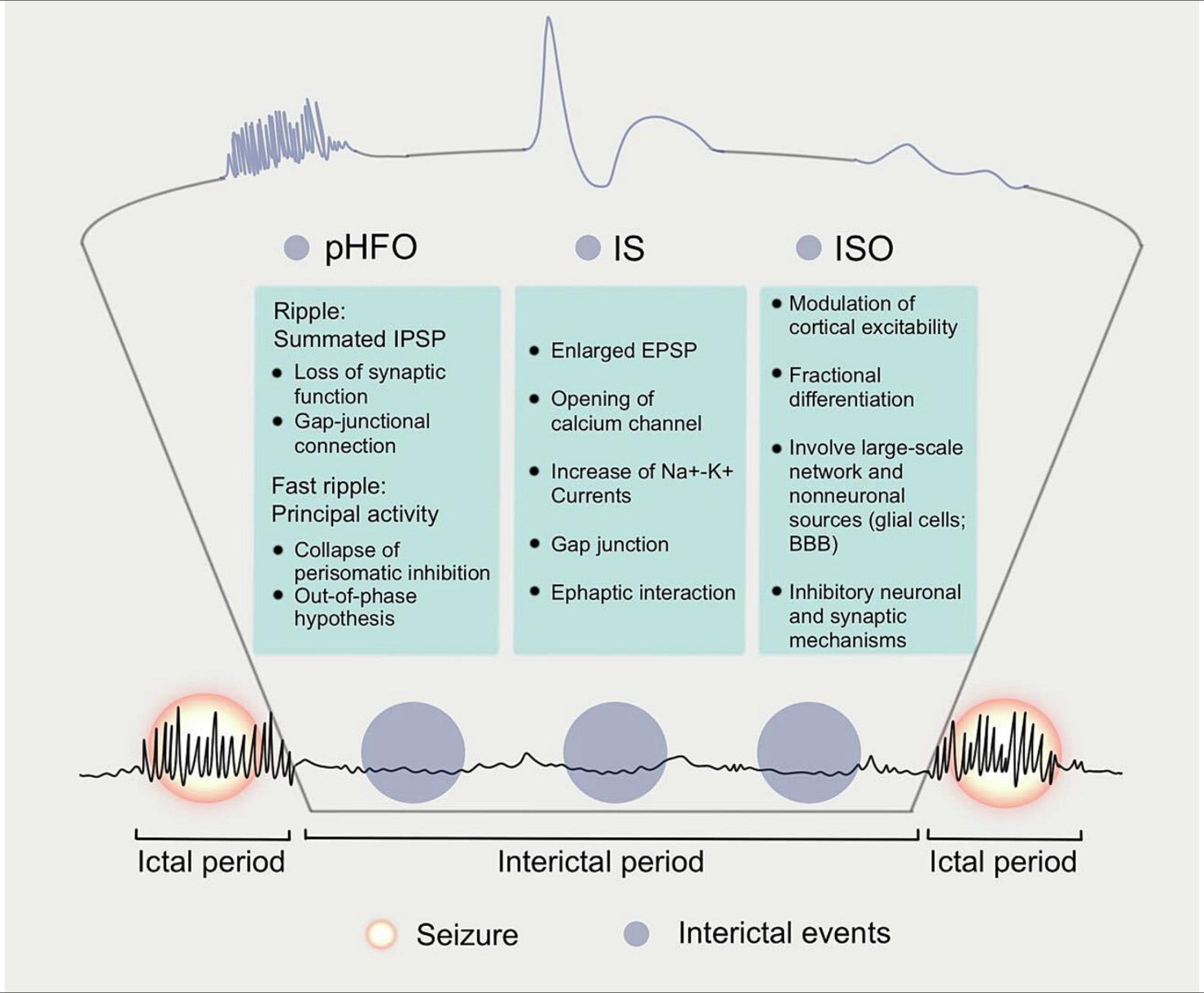
pHFO
IS
ISO
Ripple:
Summated IPSP
Loss of synaptic function
Gap-junctional connection
Fast ripple:
Principal activity
Collapse of perisomatic inhibition
Out-of-phase hypothesis
Enlarged EPSP
Opening of calcium channel
Increase of Na+-K+ Currents
Gap junction
Ephaptic interaction
Modulation of cortical excitability
Fractional differentiation
Involve large-scale network and nonneuronal sources (glial cells; BBB)
Inhibitory neuronal and synaptic mechanisms
Ictal period
Interictal period
Ictal period
Seizure
Interictal events

Presurgical evaluation

Predicting EZ or SOZ

Reflection of disease severity

Respond to drug change

Predictor of status epilepticus

SE: seizure last 30 min

Forecast of seizure occurrence

Using interictal brain activity to predict impending seizures

Established

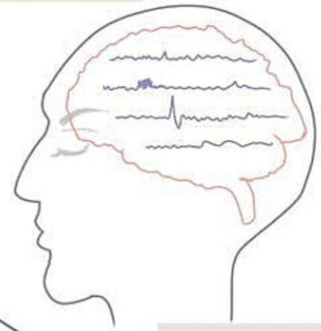

Outlook

Interictal state/oscillation -activated ensemble

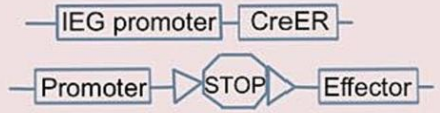

Activity-dependent techniques

Diversity and subtype differentiation

Interictal functional connectivity

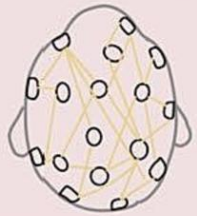

Interictal EEG-based RNS treatment

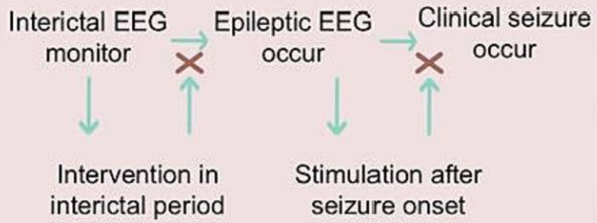

Combining analysis of
time-varying
spike rates with automated sleep staging
demonstrated that spikes in non-rapid
eye movement
sleep are more frequent and better localize se
generators
than spikes occurring in wakefulness

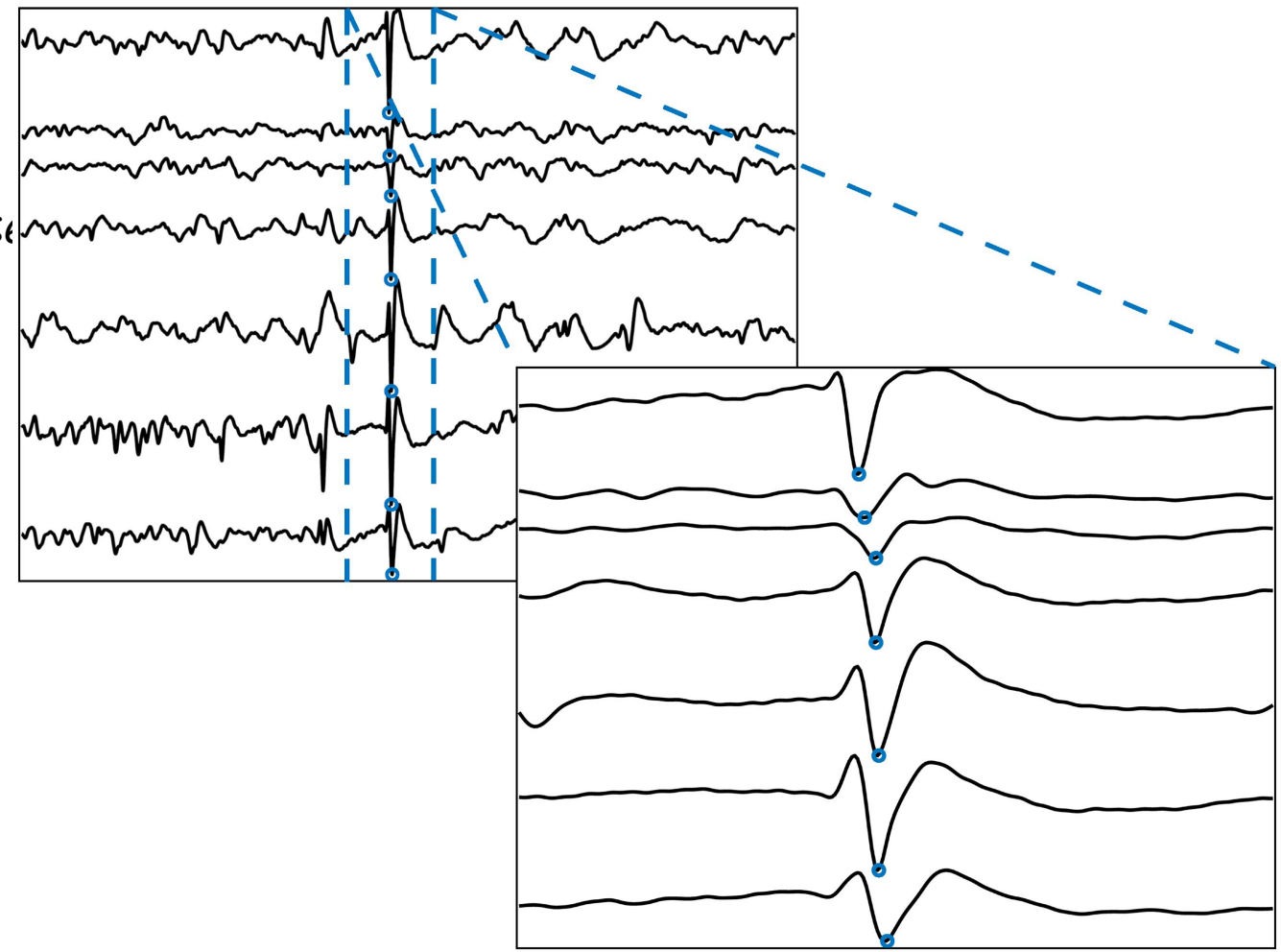

Andrade-Valenca et al.,2011
The rates and the proportion of channels with gamma and ripple fast oscillations are higher inside the SOZ, indicating that they can be used as interictal scalp EEG markers for the SOZ.

Figure 1 Patient 10: Examples of artifacts and ripple oscillations

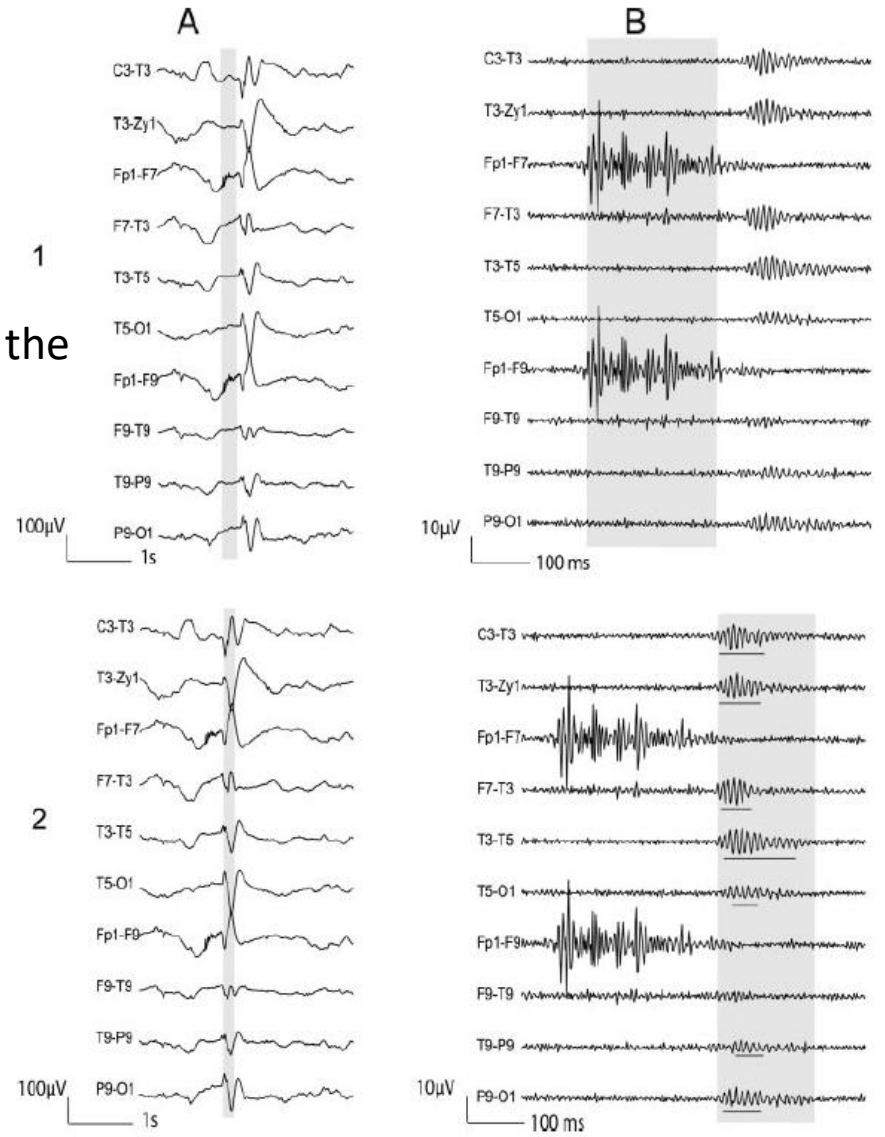

1) Short EMG bursts. 2) Ripples co-occurring with sharp wave. (A) Raw EEG. (B) EEG filtered with high-pass filter of 80 Hz. Gray section in A is expanded in time and amplitude in B. Note that for this and subsequent figures the calibration is different in the left and right part of the figure, but is the same for the top and bottom parts. Ripple oscillations are underlined. The waveform morphology of nonartifactual fast oscillations is more rhythmic and regular in amplitude and frequency than artifactual oscillations.

Figure 3 Patient 4: Examples of artifacts and gamma oscillations

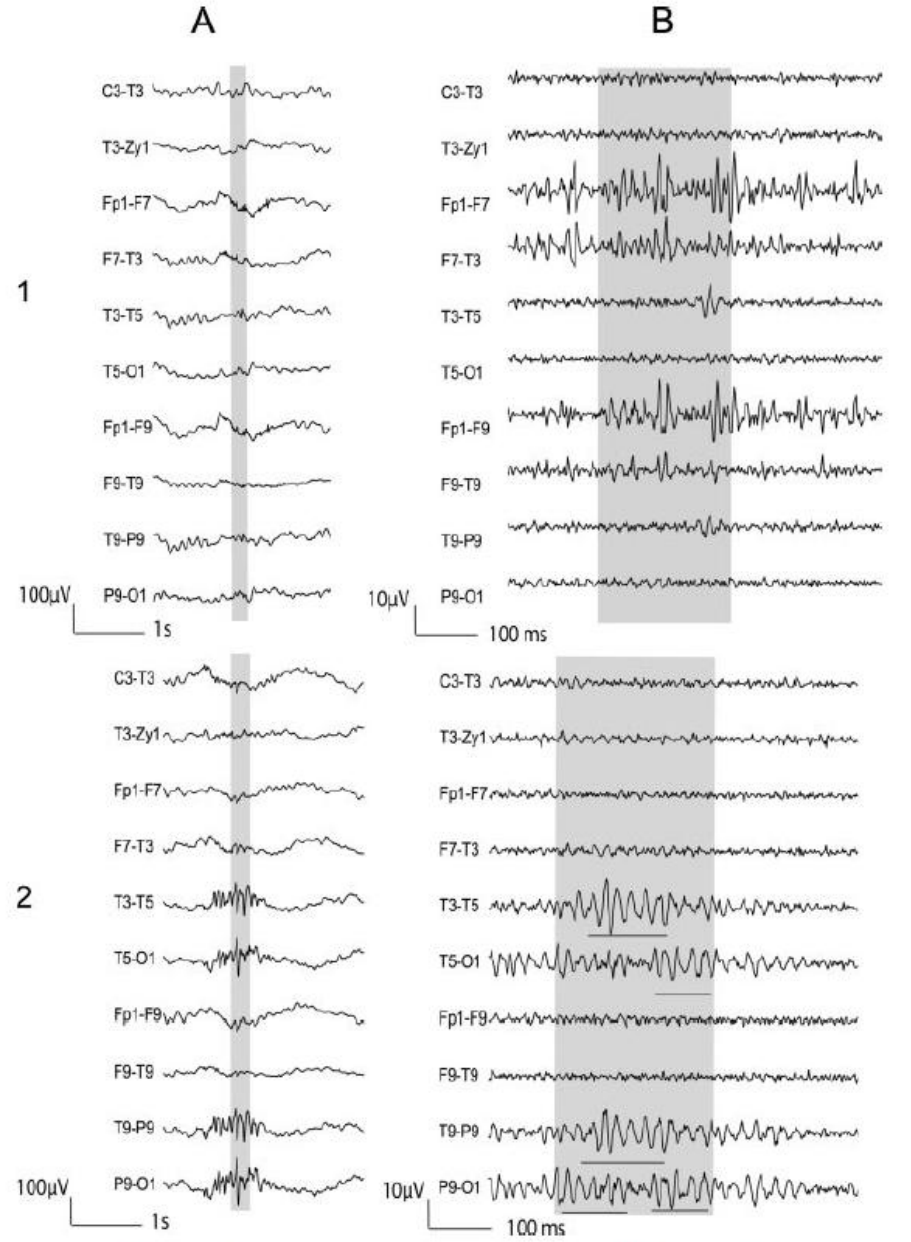

1) Short EMG bursts. 2) Gamma co-occurring with polyspikes. (A) Raw EEG. (B) EEG filtered with high-pass filter of 40 Hz. The gamma oscillations are underlined.

Спектральный анализ

Figure 2

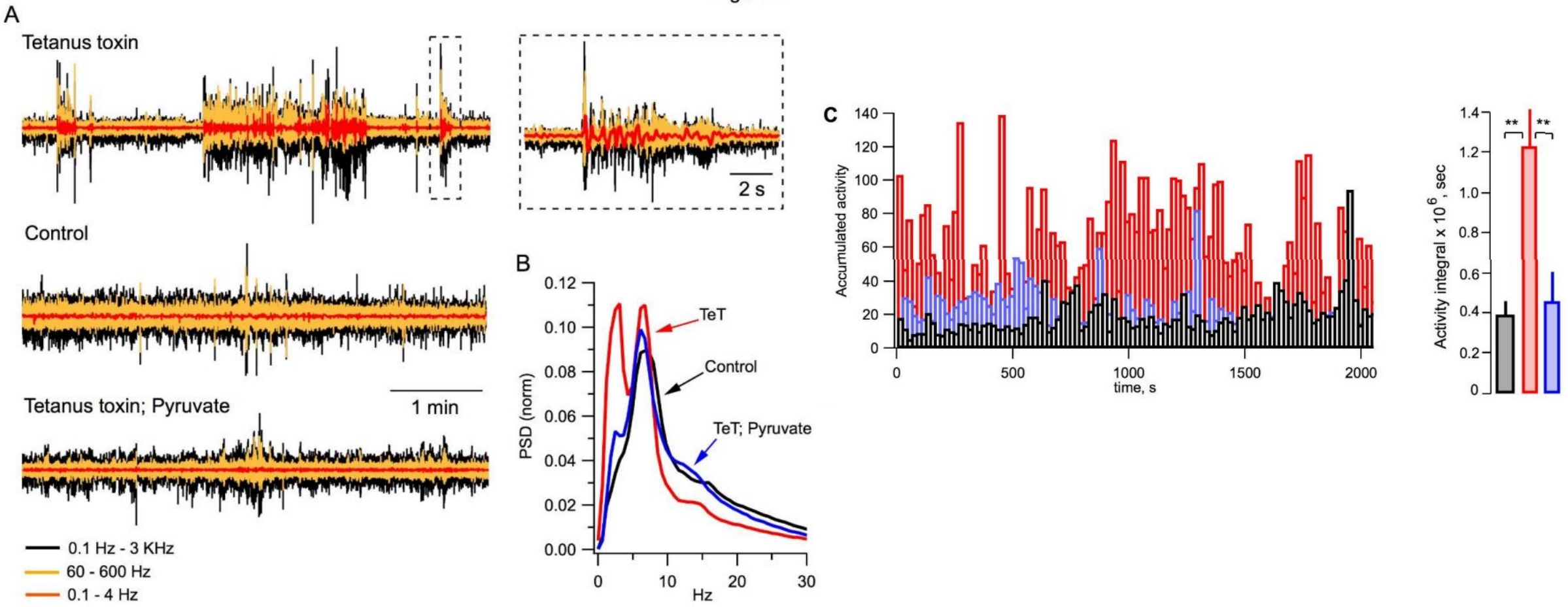
A
Tetanus toxin
Control
Tetanus toxin; Pyruvate
1 min
2 s
0.1 Hz - 3 KHz
60 - 600 Hz
0.1 - 4 Hz
B
PSD (norm)
Hz
TeT
Control
TeT; Pyruvate
C
Accumulated activity
time, s
Activity integral x 10^6, sec
**
**

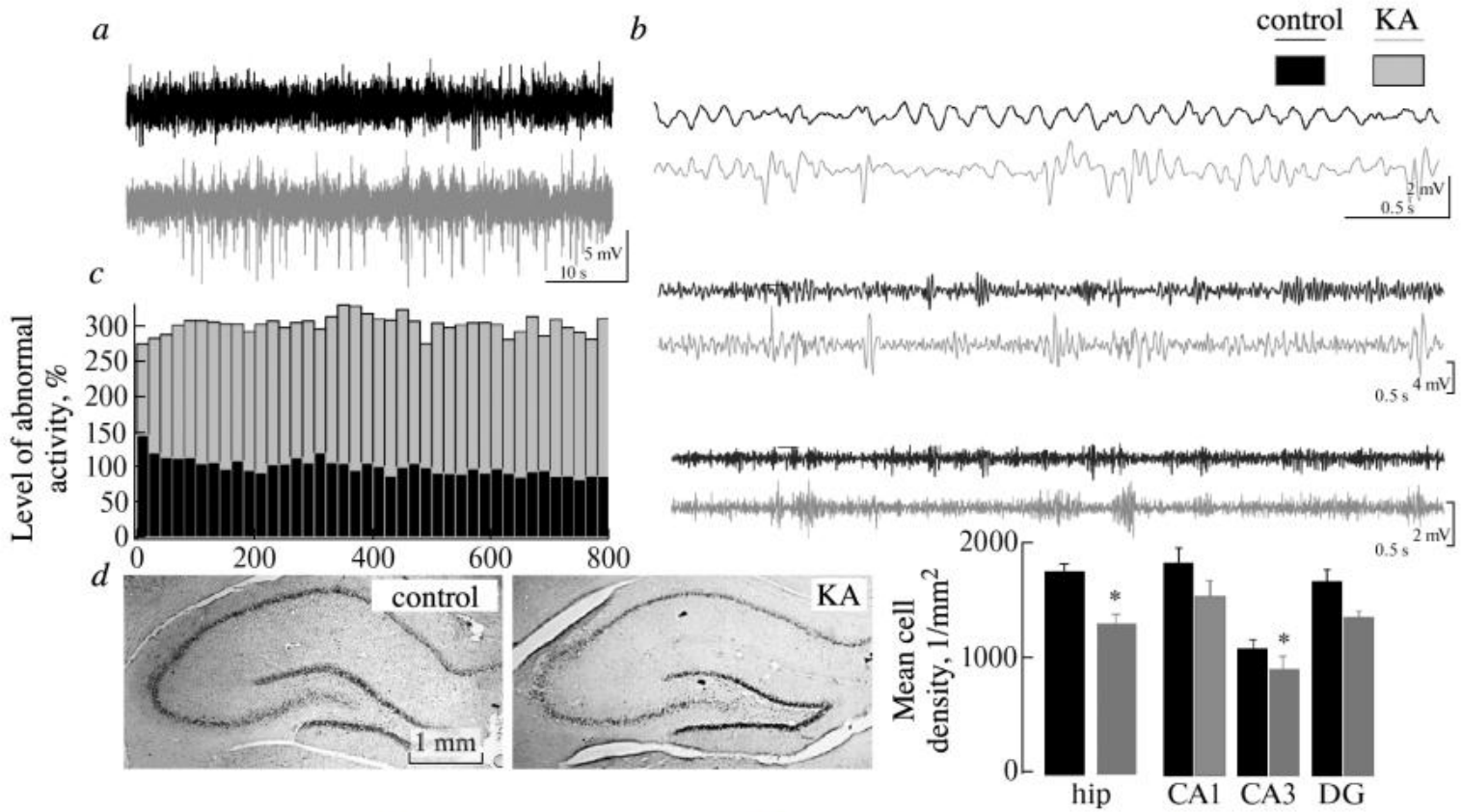

Fig. 2. Changes in the field activity and state of hippocampal tissues in the model of kainate neurotoxicity. *a*) Examples of recorded hippocampal LFP from healthy animals (controls) and in the model of kainate neurotoxicity (KA). Animals with the kainate neurotoxicity model displayed frequent high-amplitude paroxysmal events. *b*) Examples of LFP (same as in *a*) filtered in the θ (4–10 Hz, above), slow γ (25–50 Hz, middle), and fast γ (55–100 Hz, below) ranges. *c*) Total level of anomalous activity, all animals – integral of all high-amplitude (>3SD) events in hippocampal LFP. The level in controls was taken as 100%. *d*) Examples of frontal sections of the hippocampus stained by the Nissl method. Left: sections including all hippocampal fields and the dentate fascia in controls and after administration of kainic acid (KA); right: histogram showing mean cell density in the hippocampus as a whole (hip) and in separate parts of the hippocampus (CA1, CA3, DG); significant changes in cell numbers in field CA3 (*$p = 0.0483$).

Li et al.2018

MEG study.
Compared with the healthy controls, the left TLE group presented significantly increased powers in the left temporal region, whereas the right TLE group exhibited significantly increased powers in the right temporal region in the delta and theta bands.
Our results suggest that in the delta and theta bands, regional average powers in the left and right temporal regions can be taken as biomarkers for distinguishing MRI-negative TLE patients from healthy controls.

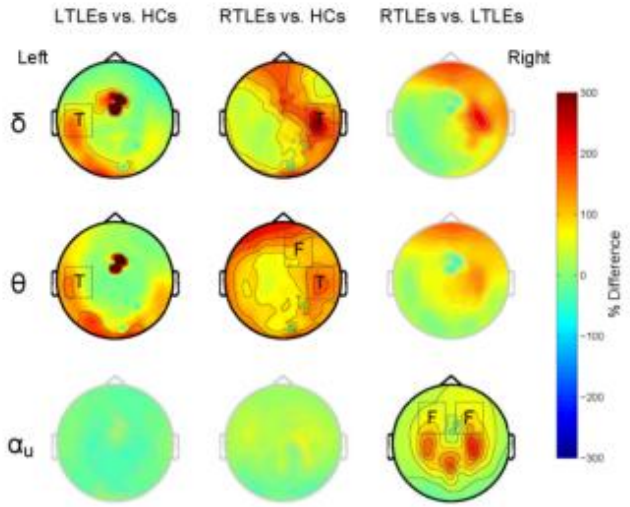

Figure 1. Regional band-power comparisons between the three groups of subjects. RTLEs = right TLEs; LTLEs = left TLEs; HCs = healthy controls; δ = delta; θ = theta; α_u = upper alpha; F = frontal; T = temporal.

In the global band power, the right TLE group presented significant increases in the delta (corrected $P = .026$) and theta (corrected $P = .015$) bands when compared with the healthy controls (Fig. 2). No significant differences between the left TLE group and the healthy controls and between the left and right TLE groups in the global band power were found for any selected frequency band.

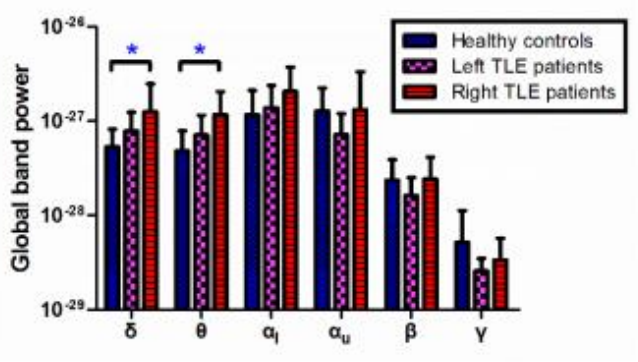

Figure 2. Global band-power comparisons between the three groups of subjects. Error bars denote standard deviations of global power. Asterisks indicate that there was a significant difference between the specified two groups using the Wilcoxon rank-sum test (two-tailed) after Bonferroni correction. δ = delta; θ = theta; α_l = lower alpha; α_u = upper alpha; β = beta; γ = gamma.

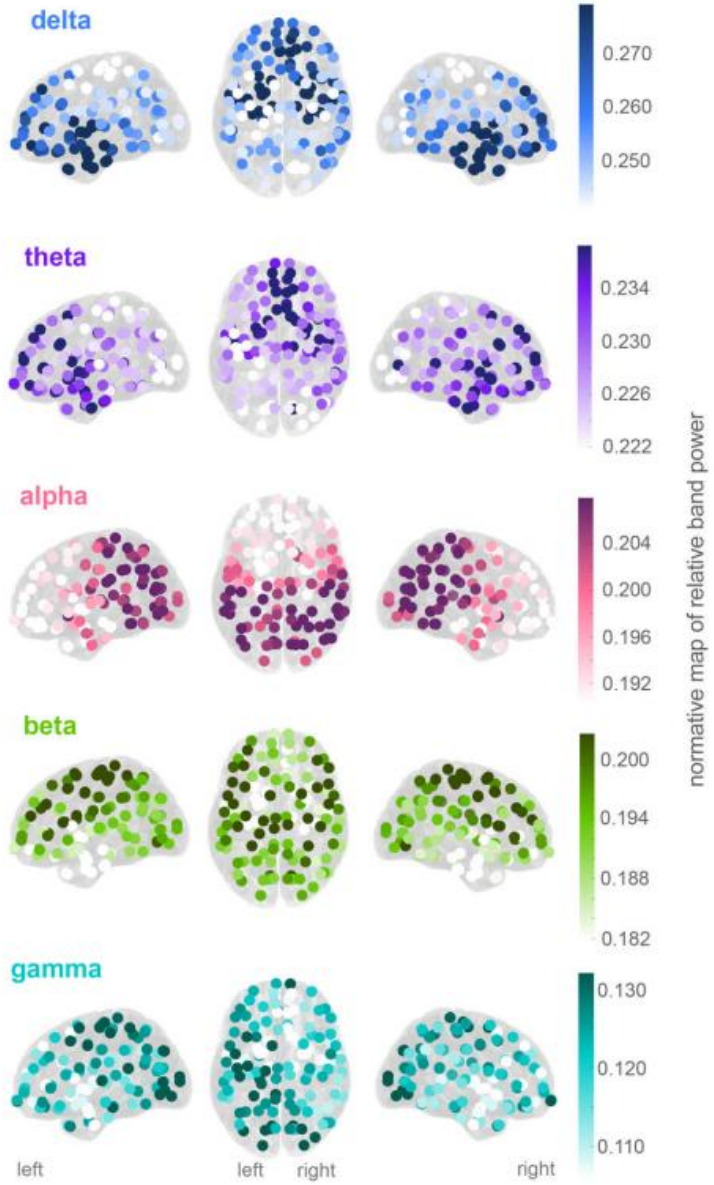

Figure 1 Normative band power varies across regions. Mean relative band power in each region for each of the five frequency bands of interest. The colour axes scale differs for each frequency band with generally higher power in lower frequencies.

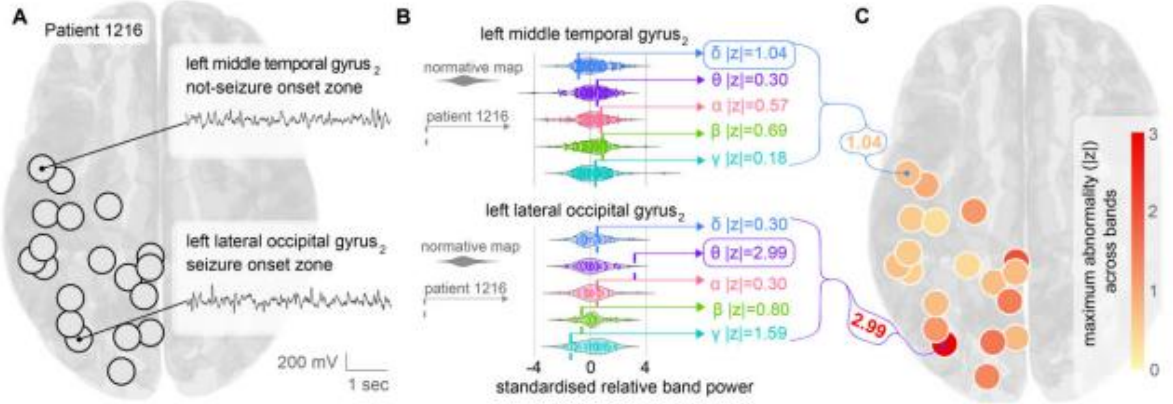

Figure 2 Normative band power as a reference to detect abnormalities in individual patients. (**A**) Visualization of the regions covered by the implanted electrodes in an example patient with epilepsy. 18 of the 128 regions were sampled by the electrode contacts in this patient (black circles). Time series from two example regions are shown that are without obvious epileptiform activity (inset). One example region (left lateral occipital gyrus 2) was the seizure onset zone in this patient. (**B**) Relative band power for each of the two regions, across each frequency band is plotted for the normative data (coloured violin plot; each point is a normative participant). Data are standardized (mean subtracted and divided by standard deviation). Relative band power z-score for Patient 1216 is plotted as a vertical dashed line on the same scale. The z-scores indicates that the left middle temporal gyrus is normal in all frequency bands (maximum absolute z = 1.04). The left lateral occipital gyrus is more abnormal in theta (maximum absolute z = 2.99) and gamma (absolute z = 1.59). (**C**) Maximum absolute z-score for each region plotted for the patient. Larger values indicate greater abnormality in any frequency band.

Kalamangalam et al. 2014 Specifically, we hypothesized that transmission of oscillatory disturbance within or close to areas of focal epilepsy would be less ‘constrained’ than over normal areas — allowing oscillatory instabilities to propagate more readily within the network — and that these changes would be detectable on scalp EEG.

Spectra from patientsshowed a noticeable left-right asymmetry in the fluctuationsof the spectral waveform (i.e., line length, that character-ized the ‘wiggliness’ of the line about its trajectory) in thecanonical , , and bands (Figs. 2 and 3), in comparison tonormal

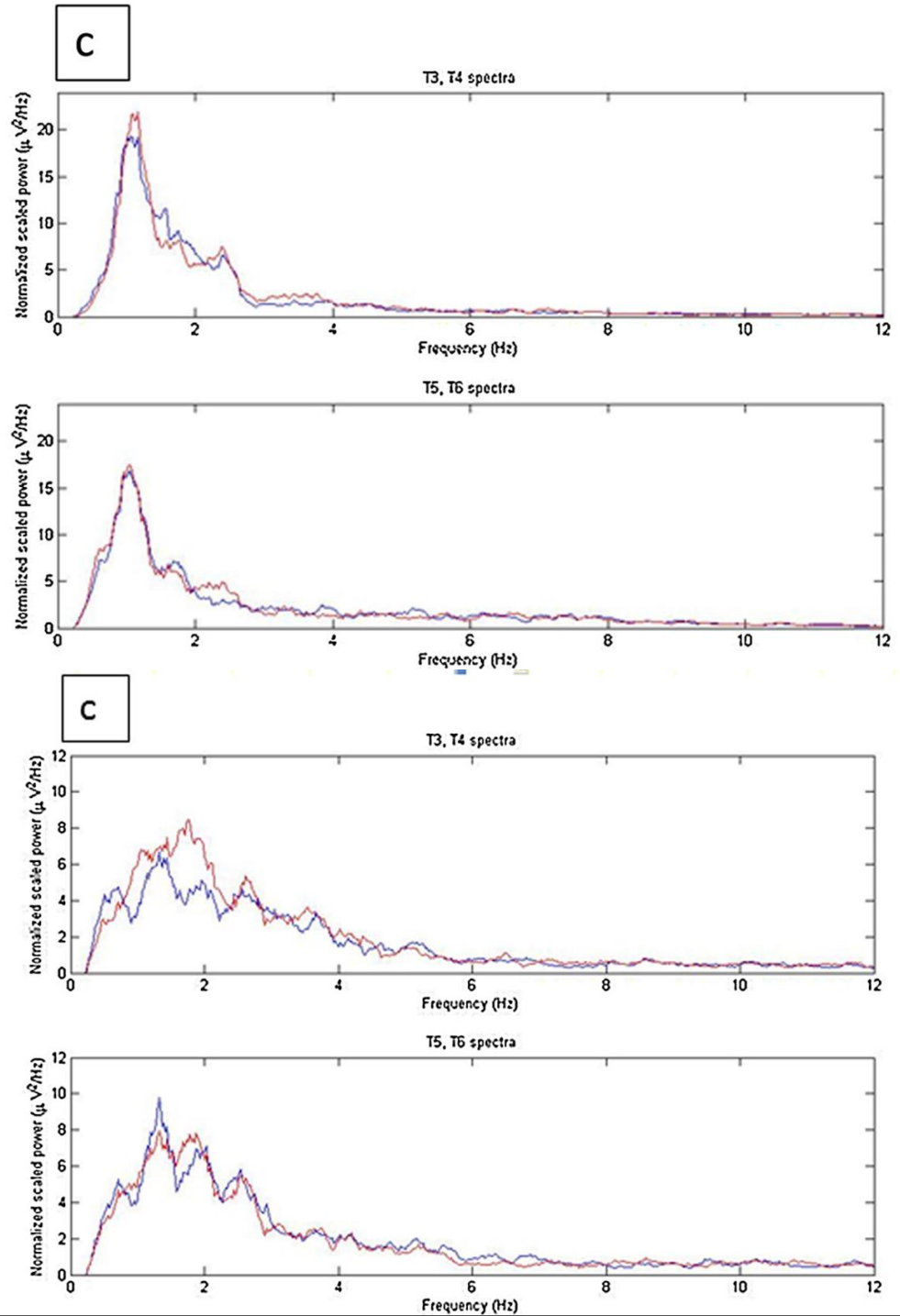

Pyrzowski et al. 2015
Zerocrossing
interval analysis is an alternative to Fourier analysis for the assessment of the rhythmic
component of EEG signals
The
identified putative epilepsy-specific markers were sensitive to the properties of the alpha rhythm and displayed weak or non-significant dependences on the number of antiepileptic drugs (AEDs) taken by the patients

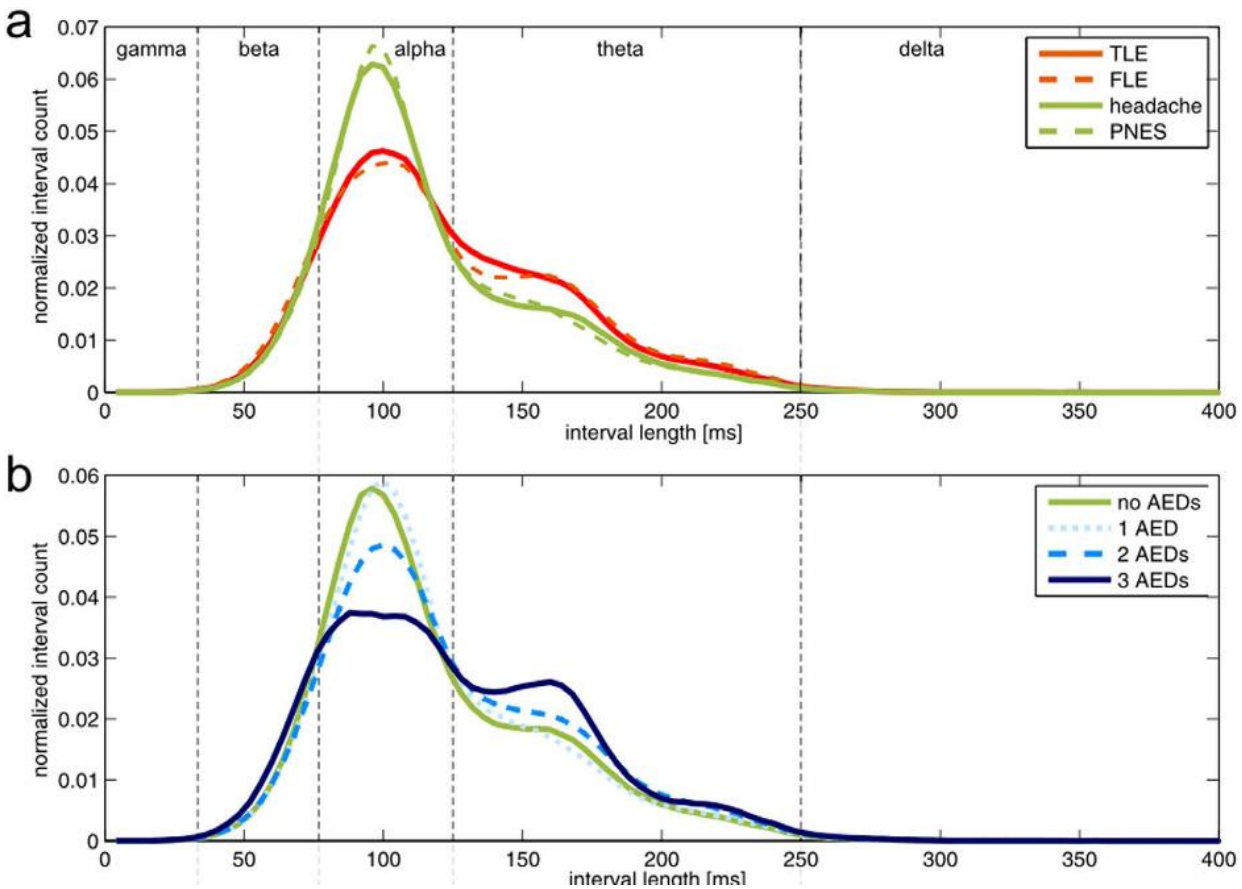

Фазово-амплитудная модуляция

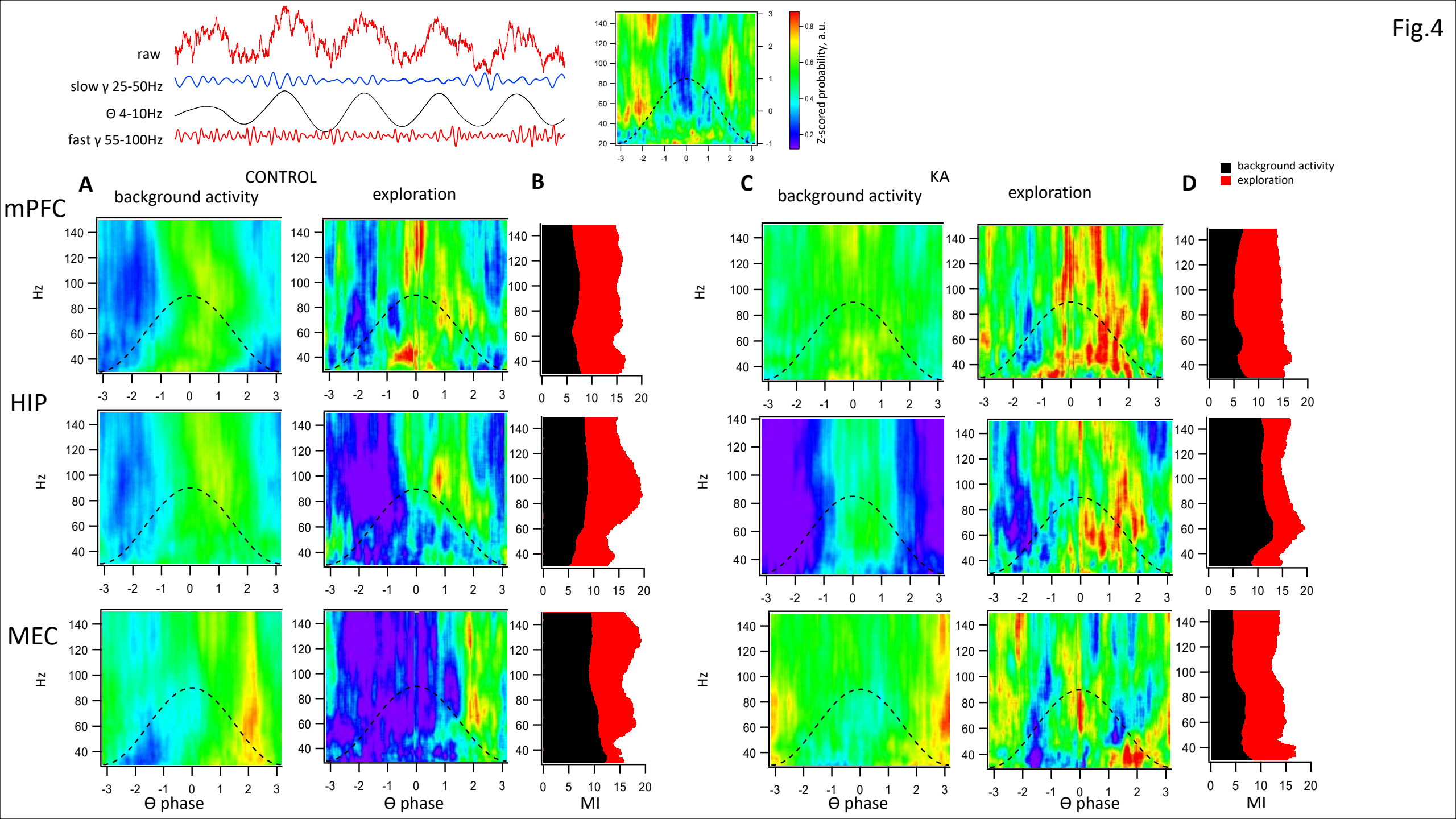
raw
slow γ 25-50Hz
Θ 4-10Hz
fast γ 55-100Hz
Z-scored probability, a.u.
A
CONTROL
background activity
exploration
B
C
KA
background activity
exploration
D
background activity
exploration
mPFC
HIP
MEC
Hz
Θ phase
MI

Fig.4

Ma et al., 2021

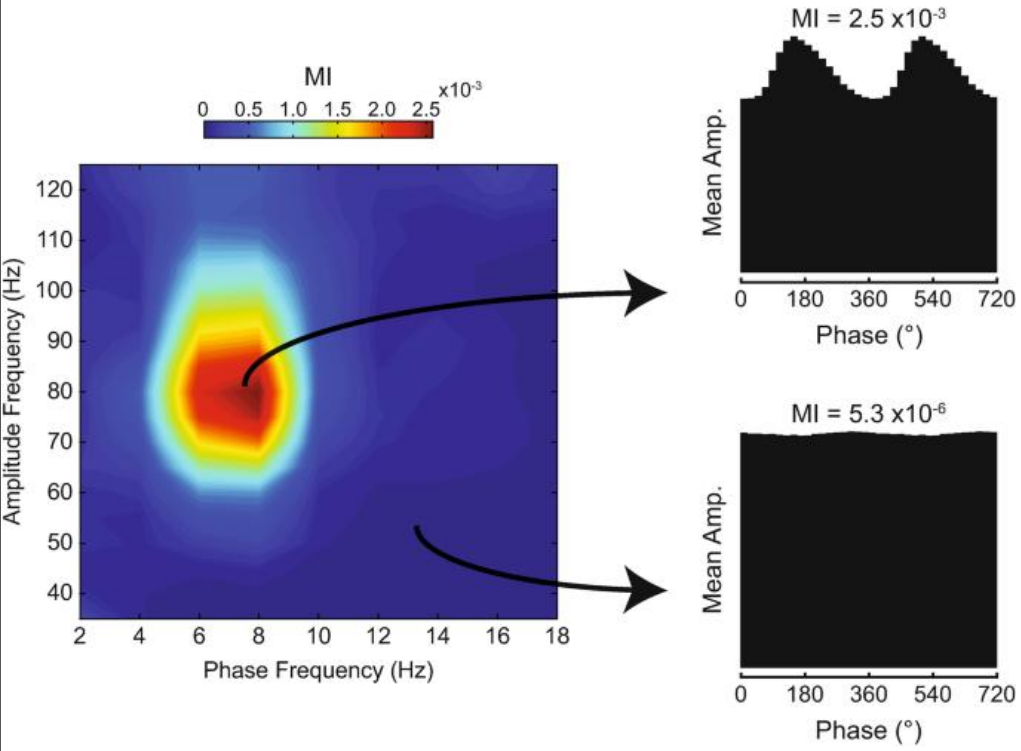

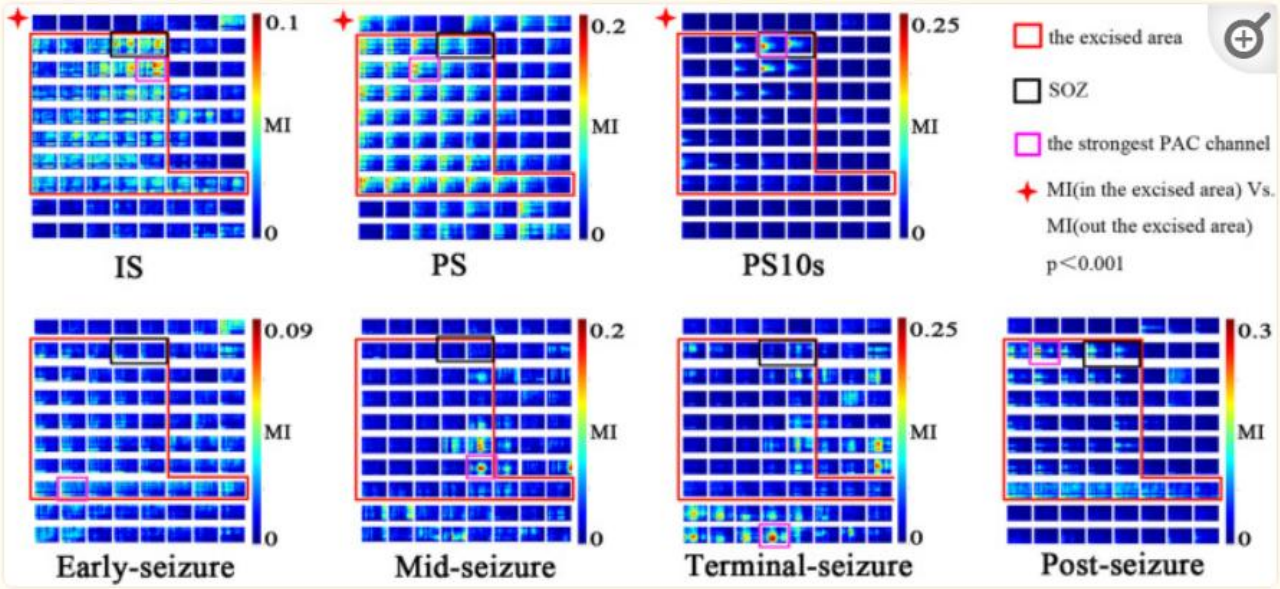

Figure 4

Spatial specificity of PAC. Modulation was computed in 10-s windows at different seizure periods (IS, PS, PS10, early-seizure, mid-seizure, terminal-seizure, post-seizure). The MI co-modulograms of all channels were arranged in turn in each sub-figure. The scales were indicated by the color bar on the right side of the sub-figure. The red rectangle is the excised area; The black rectangles is SOZ; The purple rectangles is the strongest PAC channel. This figure shows that the strong PAC in the IS, PS, PS10 periods was more concentrated on the resection margin. Once seizure begined, the strong PAC gradually subsided from SOZ to surrounding general resection area, and gradually translocated to the unresection area. In the post-seizure period, the strong PAC channels returned to the resected area. During the IS and PS period, the strongest PAC channel was usually located in resection margin very near but not SOZ; in the PS_{10}, it was often located in the SOZ.

Amiri et al.2016
PAC between high and low frequency rhythms was found to be significantly stronger in the SOZ compared to normal regions. Also, the coupling was generally more elevated in spiking channels outside the SOZ than in normal regions.

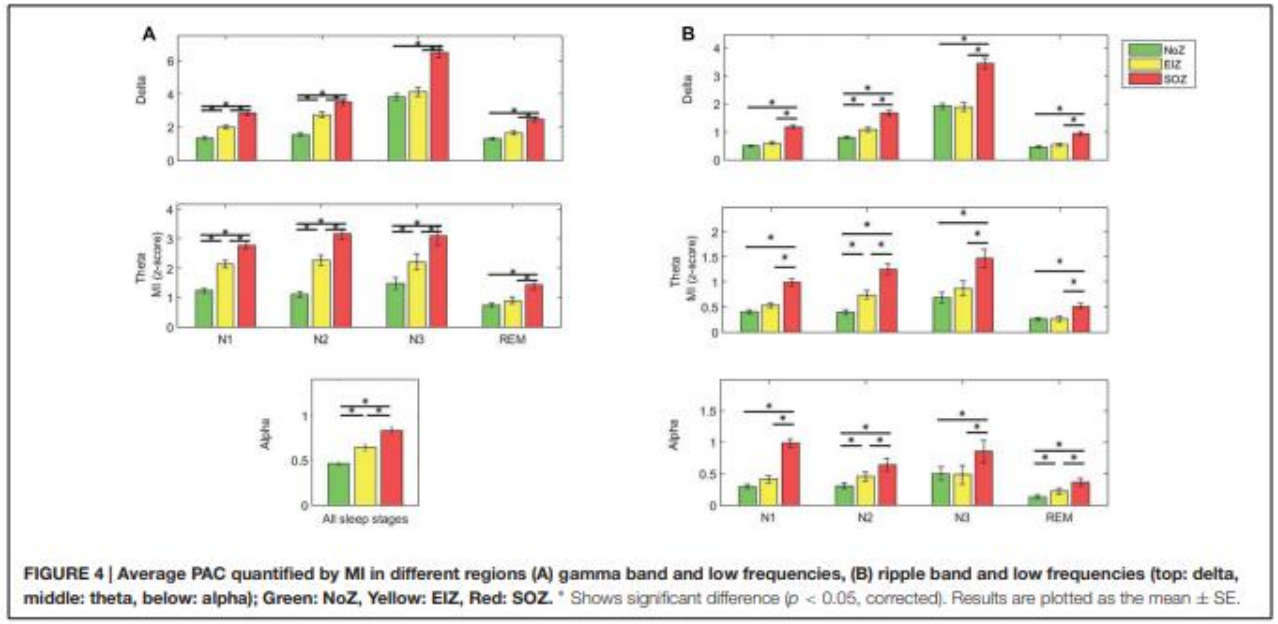

FIGURE 4 | Average PAC quantified by MI in different regions (A) gamma band and low frequencies, (B) ripple band and low frequencies (top: delta, middle: theta, below: alpha); Green: NoZ, Yellow: EIZ, Red: SOZ. * Shows significant difference ($p < 0.05$, corrected). Results are plotted as the mean ± SE.

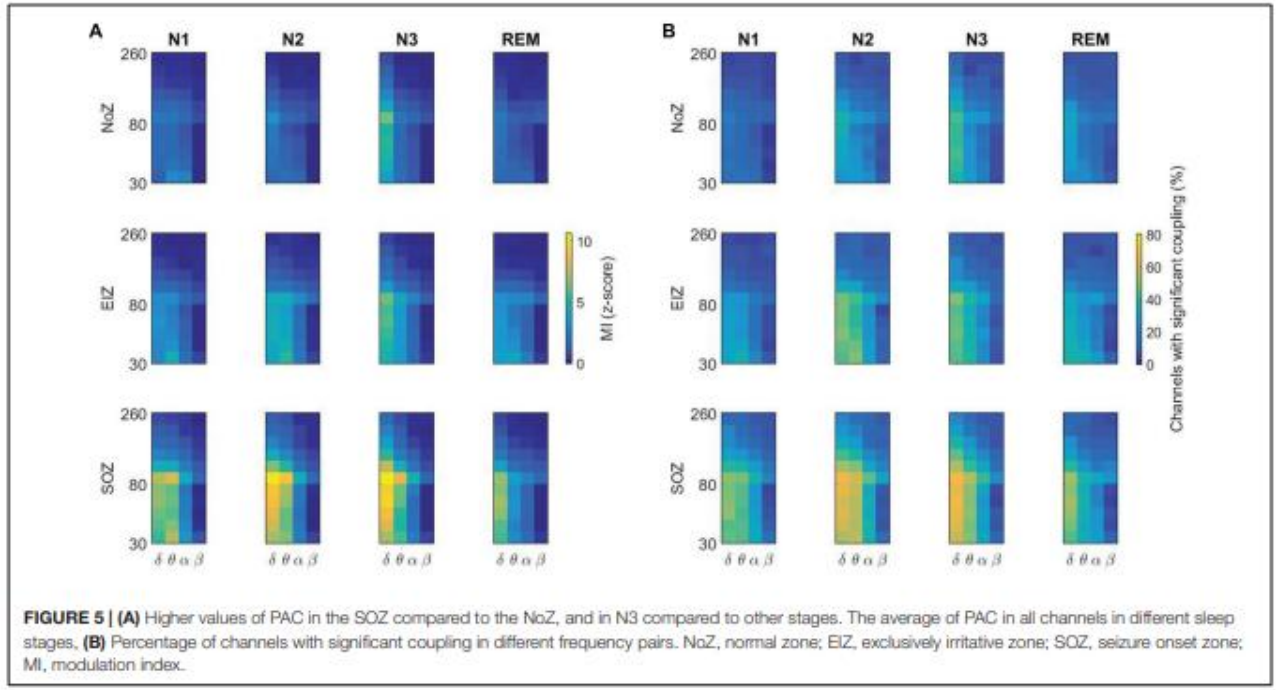

FIGURE 5 | (A) Higher values of PAC in the SOZ compared to the NoZ, and in N3 compared to other stages. The average of PAC in all channels in different sleep stages, **(B)** Percentage of channels with significant coupling in different frequency pairs. NoZ, normal zone; EIZ, exclusively irritative zone; SOZ, seizure onset zone; MI, modulation index.

Gunnarsdotir 2022

We developed an algorithm that identifies two groups of nodes from the interictal iEEG network: those that are continuously inhibiting a set of neighbouring nodes (‘sources’) and the inhibited nodes themselves (‘sinks’).

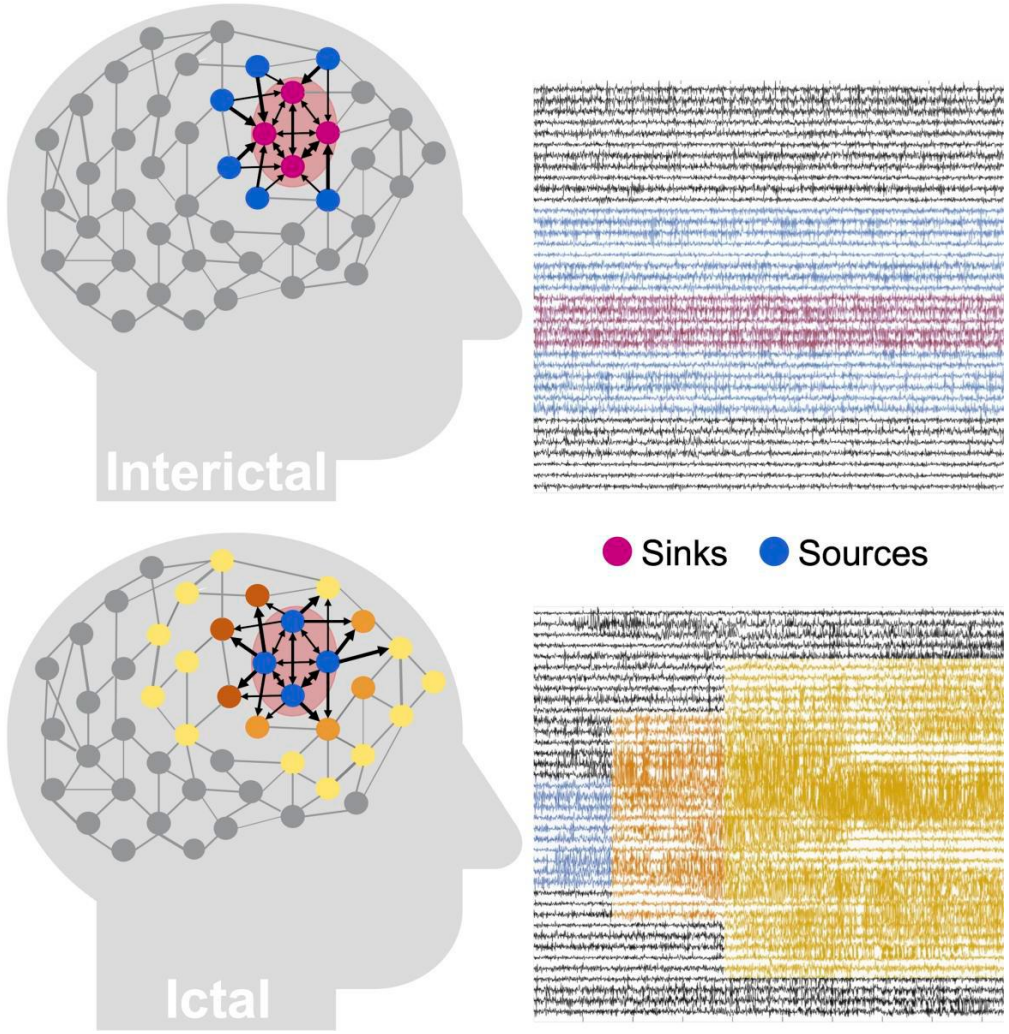

1. Сбор данных и построение карт нормальной активности мозга в стандартных отведениях:

А) карта спектральной мощности и локализации источников ритмической активности

Б) карта когерентности и функциональной связанности отведений

В) карта кросс-частотной модуляции

2. Анализ патологической ЭЭГ с выявлением абнормальной активности и отклонений от нормативных карт

3. Разработка автоматизированного алгоритма выявления патологической активности связанной с гипервозбудимостью.

HFOs are extracted by amplifying the suitably filtered EEG signal and refer to distinct types of brain activity occurring in a frequency band ranging from 80 Hz to 600 Hz and have been typically separated into ripples (80–250 Hz) and fast ripples (FRs: 250–600 Hz)

Moreover, FRs appear to correlate with reduced hippocampal volumes and neuronal loss both in experimental models (Bragin et al., 2002a; Foffani et al., 2007) and in human TLE (Ogren et al., 2009; Staba et al., 2007).

ISs can be distinguished from non-epileptic sharp waves that are putatively sustained by physiologically bursting neurons by qualitative and quantitative criteria and have characteristics as follows: (1) Di- or tri-phasic wave with sharp or spiky morphology; (2) different wave duration than the ongoing background activity; (3) asymmetry of the waveform; (4) followed by a slow after-wave; (5) the background activity is disrupted by the presence of the ISs; and (6) voltage map with the distribution of negative and positive potentials suggesting a source in the brain corresponding to a radial, oblique, or tangential orientation of the source (Kane et al., 2017); while nonepileptic sharp waves are irregular, show a complex morphology, are smaller in amplitude and have a longer duration than ISs (de Curtis and Avanzini, 2001).

the majority of ISs were traveling waves, traversing the same path as ictal discharges during seizures and with a fixed direction relative to seizure propagation and most ISs were bidirectional, with one predominant and a second, less frequent antipodal direction (Smith et al., 2022).

Slow wave activities (SWAs), designated as low-frequency oscillations, could include frequencies in the delta power range (0.5–4 Hz) and very low-frequency activity that is typically called infraslow activities (<0.1 Hz) (de Goede and van Putten, 2019; Lundstrom et al., 2019).

HFOs are believed to originate from transient synchronization of neuronal populations (Engel and da Silva, 2012; Engel Jr et al., 2009) or disinhibited neuronal networks (Zijlmans et al., 2011), leading to highly synchronized neuronal activity over an area of brain tissue associated with normal and pathological brain functions. Evidence suggests that pathologic HFOs (pHFOs) in the ripple band represent summated synchronous inhibitory postsynaptic potentials (IPSP) generated by interneurons regulating the activity and

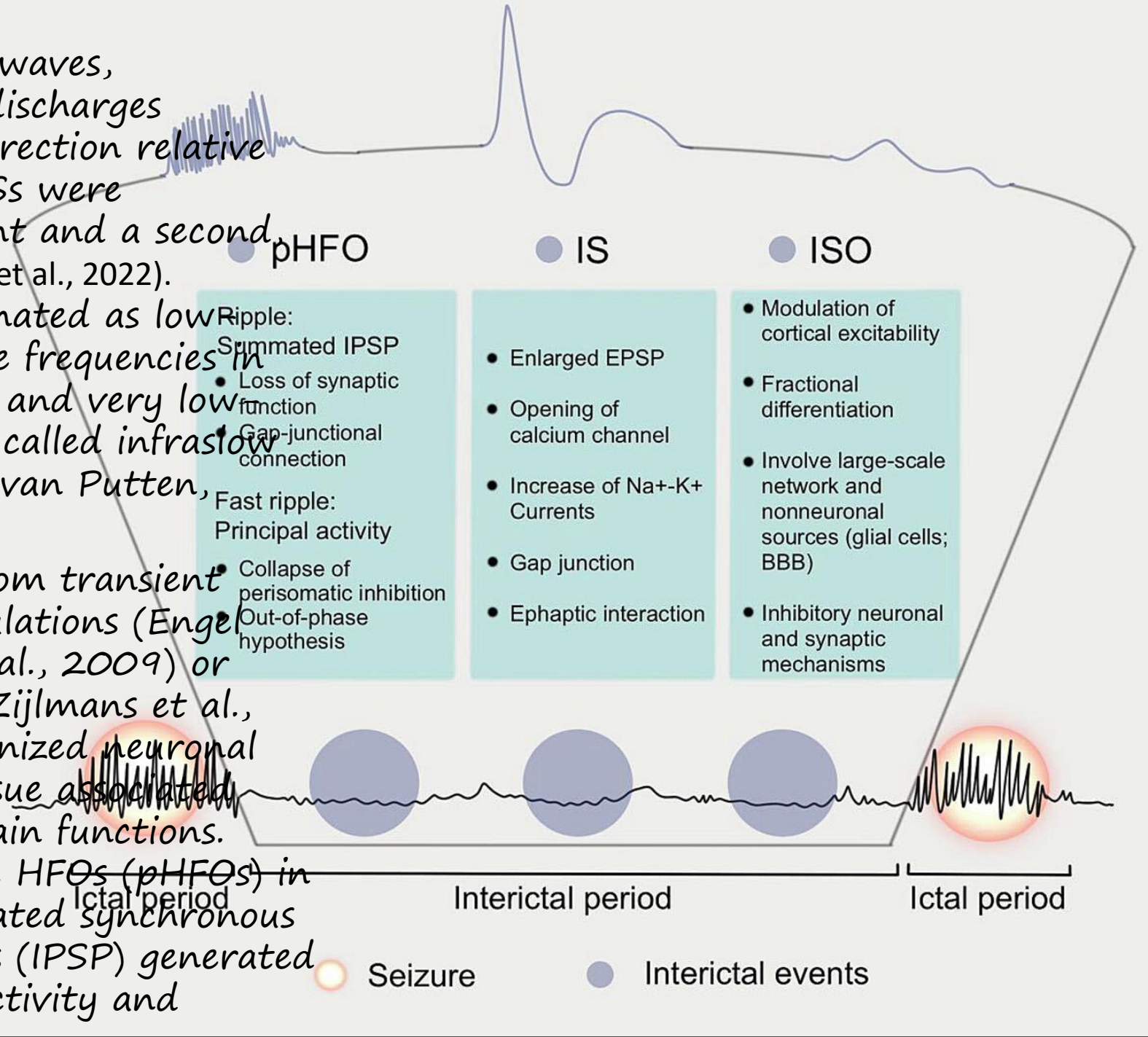

revealed network markers of seizures from short epochs of the interictal resting state, suggesting that the causal network properties that drive seizure onset and propagation are observable even in the absence of seizures and interictal events (e.g., ISs) which further illustrated that the epileptic brain has an enduring trait to produce seizures (Woldman et al., 2020). Similarly, Coito et al. revealed that directed functional networks inferred from interictal EEG may be used to diagnose TLE in the absence of ISs and thus these resting-state connectivity alterations could constitute an important biomarker of TLE (Coito et al., 2016).

Lundstrom et al. showed that a combination of interictal biomarkers including the ISOs, ISs rate, and HFOs rate correctly predicted whether the left, right, both, or neither temporal lobes were involved for almost 90% of patients (Lundstrom et al., 2021).

Lai et al. 2023